Electronic Supplementary Material (ESI) for RSC Advances.
This journal is © The Royal Society of Chemistry 2019

Electronic Supplementary Material (ESI) for Chemical Communications
This journal is © The Royal Society of Chemistry 2019

Electronic Supplementary Information

$Ru_xSe@MoS_2$ hybrid as a highly efficient electrocatalyst toward hydrogen evolution reaction

Qi Chen,[a, b] Kefeng Wang, [b]* Jingjing Qin,[b] Songzhu Wang,[b] Wei Wei,[b] Jingge Wang, [c] Qi Shen,[c] Peng Qu [b], Daosheng Liu [a]*

[a] College of Chemistry, Chemical Engineering and Environmental Engineering, Liaoning Shihua University, Fushun 113001, Liaoning, China

[b] Henan Engineering Center of New Energy Battery Materials, Henan Key Laboratory of Biomolecular Recognition and Sensing, College of Chemistry and Chemical Engineering, Shangqiu Normal University, Shangqiu 476000, Henan, China

[c] School of Physics and Engineering, Henan University of Science and Technology, Luoyang 471023, China

[d] College of Chemistry and Molecular Engineering, Zhengzhou University, Zhengzhou 450001, China

Experimental

Materials

Na_2MoO_4, thiourea, $RuCl_3$ and Se powder were purchased from Energy Chemical Ltd. (Shanghai, China). Hydrazine hydrate (85 wt%) and KOH were purchased from Aladdin Ltd. (Shanghai, China). All chemical reagents used were of analytical grade and used without further purification. Carbon fiber paper (CFP) was bought from Shanghai Hesen Corp. Commercial 20% Pt/C catalysts were purchased from Shanghai Macklin Biochemical Co., Ltd.

Synthesis of MoS_2 nanosheets on carbon fiber paper

Prior to the synthesis, the carbon fiber paper was cut into small pieces (3 cm×1.5 cm) and then washed with ultrapure water, ethanol and acetone by ultrasonication, respectively. The cleaned carbon fiber papers were dried at room temperature before further use. MoS_2 nanosheets were grown on the carbon fiber paper through a hydrothermal reaction. Typically, 1 mmol Na_2MoO_4 and 4 mmol thiourea were dissolved in 30 mL ultrapure water by stirring. The mixture solution was transferred into a 50 mL Teflon−lined autoclave, and a piece of carbon fiber paper was immersed in. Then the autoclave was put into a oven and kept at 200 °C for 24 h. After naturally cooling down to room temperature, the carbon fiber paper was taken out and washed thoroughly with ultrapure water and ethanol, and then dried at room temperature.

Synthesis of $Ru_xSe@MoS_2$

0.042 g Se powder and 0.0363 g $RuCl_3$ were mixed in deionized water (35 mL). After vigorous stirring for 10 min, 2 mL hydrazine hydrate (85 wt%) was dropped into the above solution under constant stirring. The resulting solution was transferred into a 50 mL Teflon−lined autoclave, and the carbon fiber paper covered with MoS_2 nanosheets was immersed into the solution. Then the autoclave was sealed and maintained at 120 °C for 12 h. After naturally cooled to room temperature, the carbon fiber paper was taken out and washed thoroughly with deionized water and ethanol, and finally dried in vacuum at 60 °C overnight.

Material characterizations

X-ray diffraction (XRD) patterns were recorded at room temperature on a Bruker D8 Advance X-ray diffractometer using a Cu Kα radiation (λ=1.5416 Å) with 2θ scan range between 5° and 80°. The surface morphology of the samples was investigated by field-emission scanning electron microscopy (FESEM, FEI Quanta FEG 250) and Transmission electron microscopy (TEM, FEI Tecnai G2 F20). X-ray photoelectron spectroscopy (XPS) measurements were carried out with a ThermoFisher K-Alpha X-ray photoelectron spectrometer with an Al Kα source. All the binding energies were calibrated to the standard C 1s emission signal (284.8 eV) of the contaminant carbon during the measurement.

Electrochemical measurements

20% Pt/C catalysts were loaded on carbon fiber paper (CFP) through a drop-casting method. Briefly, 10 mg of the catalyst were dispersed in 480 μL of water–ethanol solution at volume ratio of 250:230. Then 20 μL of Nafion solution (5 wt%, DuPont) was added. The obtained mixture was ultra-sonicated for 3 h to form a homogenous ink. Then 50 μL catalyst ink was dropped onto a piece of carbon fiber paper (CFP, 1 cm×1cm) and left to dry at room temperature overnight.

The electrochemical measurements were performed using a standard three-electrode cell system with a CHI660E electrochemical workstation. The high-purity N_2-saturated 0.5 M H_2SO_4 and 1 M KOH solution were used as the electrolytes. In the basic media, a Hg/HgO electrode and a graphite rod were used as the reference electrode and counter electrode, respectively. The polarization curves for HER were measured with a potential window of -0.8 V~-1.6 V vs Hg/HgO at a scan rate of 2 mV/s. All the potentials were referenced to a reversible hydrogen electrode (RHE) using $E_{\mathrm{RHE}} = E_{\mathrm{Hg/HgO}} + 0.935$. In the acidic electrolyte, an Ag/AgCl (saturated KCl) was used as the reference electrode. The polarization curves for HER were measured with a potential window of 0.1 V~-0.8 V vs Ag/AgCl at a scan rate of 2 mV/s. All the potentials were converted to the RHE using $E_{\mathrm{RHE}} = E_{\mathrm{Ag/AgCl}} +0.197$. In order to reveal the intrinsic electrocatalytic behavior of the catalysts, a 90% IR compensation was applied to all the polarization curves based on the ohmic resistance of the solution determined by electrochemical impedance spectroscopy (EIS). EIS measurements were carried out with a frequency range of 100 mHz to 100 kHz and an amplitude of 5 mV. Z-view software was used to fit the EIS spectra. The long-term stability of the catalyst was evaluated by continuously cyclic voltammetry (CV) measurement between -0.8 V~ -1.3 V (vs Hg/HgO) in basic media and 0.1~-0.5 V (vs Ag/AgCl) in acidic media for 1000 cycles at a scan rate of 100 mVs^{-1}, and the polarization curves before and after CV measurement were recorded. Chronopotentiometry test was conducted at the corresponding potential to deliver a current density of -20 mA cm^{-2} to monitor the long-term potential-time response during the HER process.

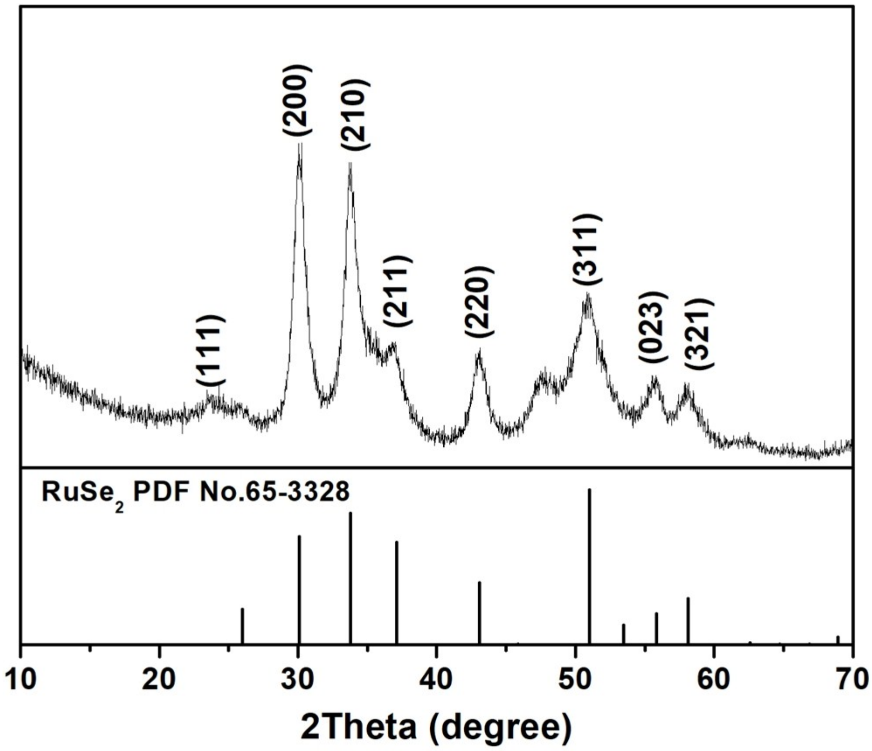

Figure S1 XRD pattern of Ru$_x$Se calcinated at 400 ^oC and the standard pattern for crystalline RuSe$_2$ (PDF No. 65-3328).

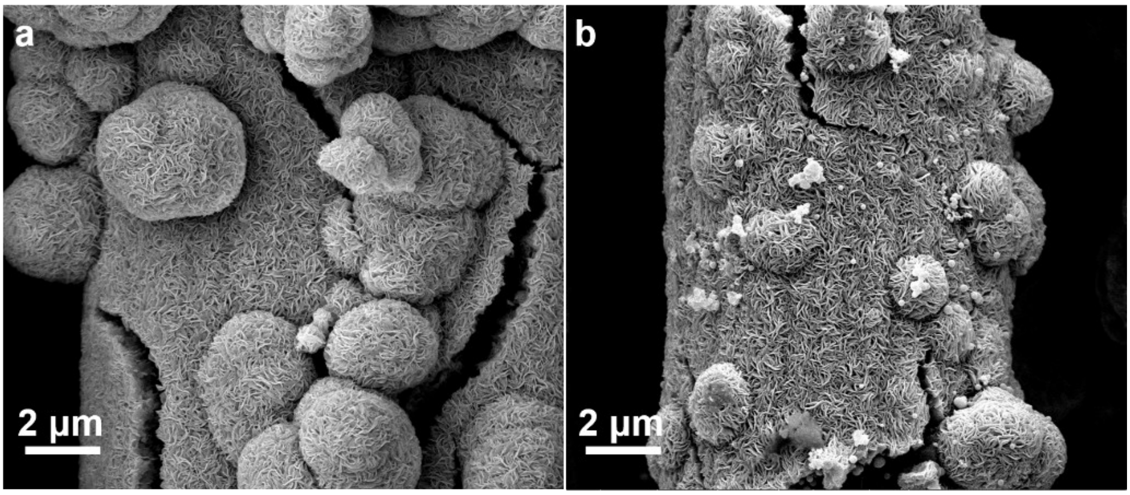

Figure S2 SEM images of MoS$_2$ and Ru$_x$Se@MoS$_2$, indicating the nanoflowers grown on the vertically aligned nanosheets.

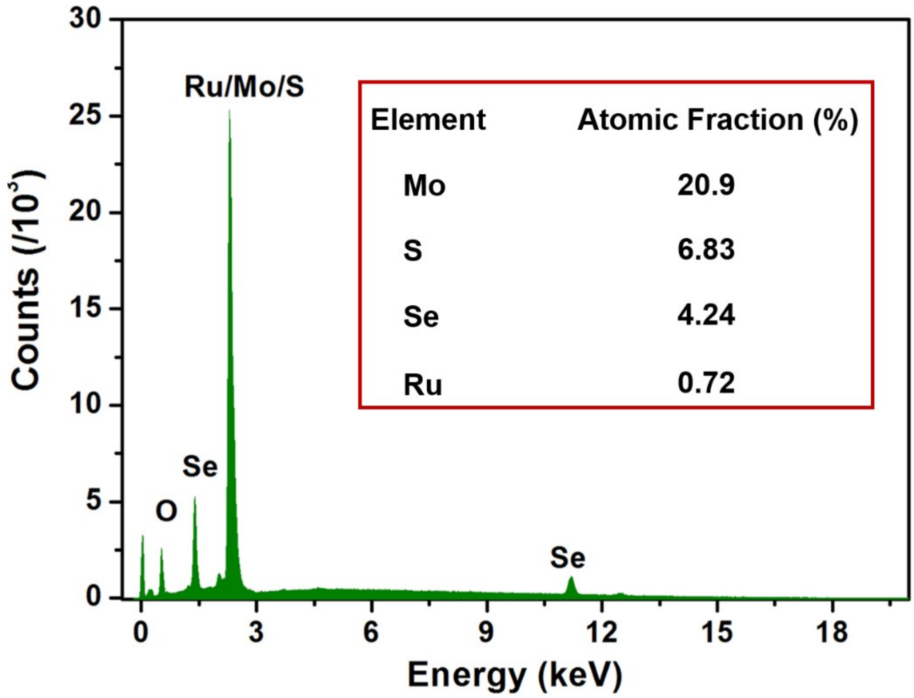

Figure S3 EDX spectrum of Ru$_x$Se@MoS$_2$ and the atomic fraction of different elements

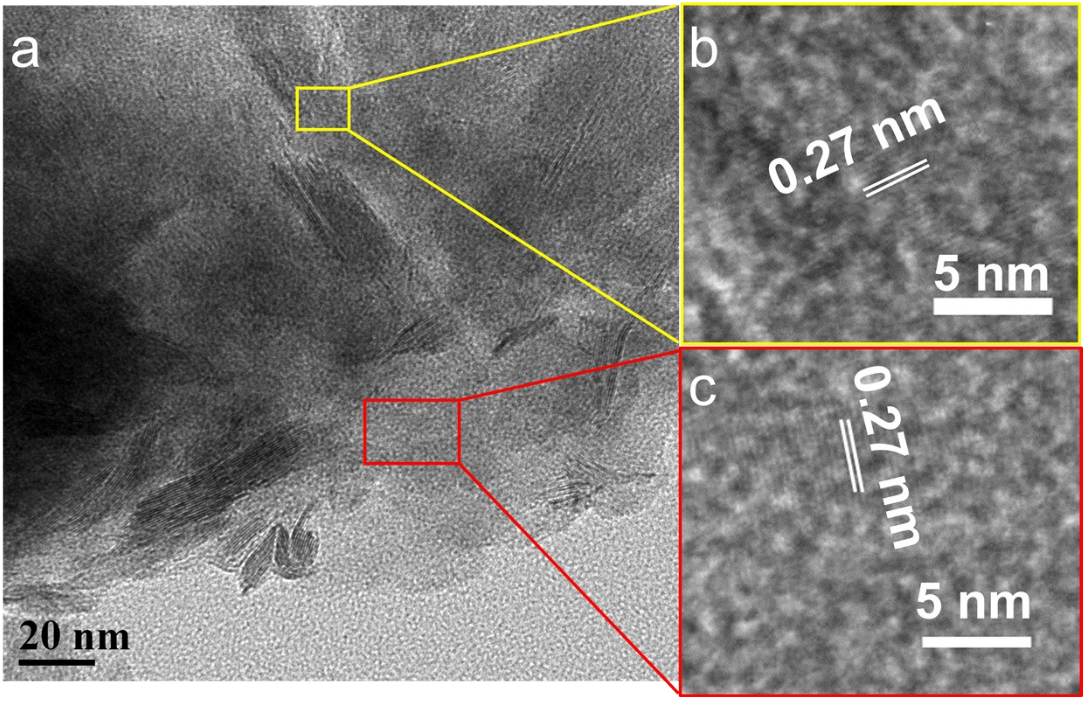

Figure S4 HRTEM image (a) of Ru$_x$Se@MoS$_2$ and two magnified images (b, c) to illustrate the interplanar space of 0.27 nm corresponding to (100) plane of 2H-MoS$_2$.

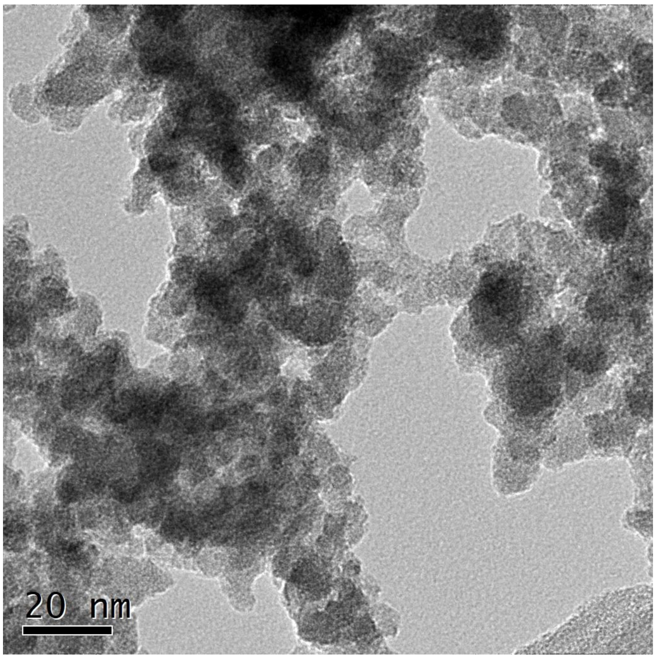

Figure S5 TEM image of Ru_xSe

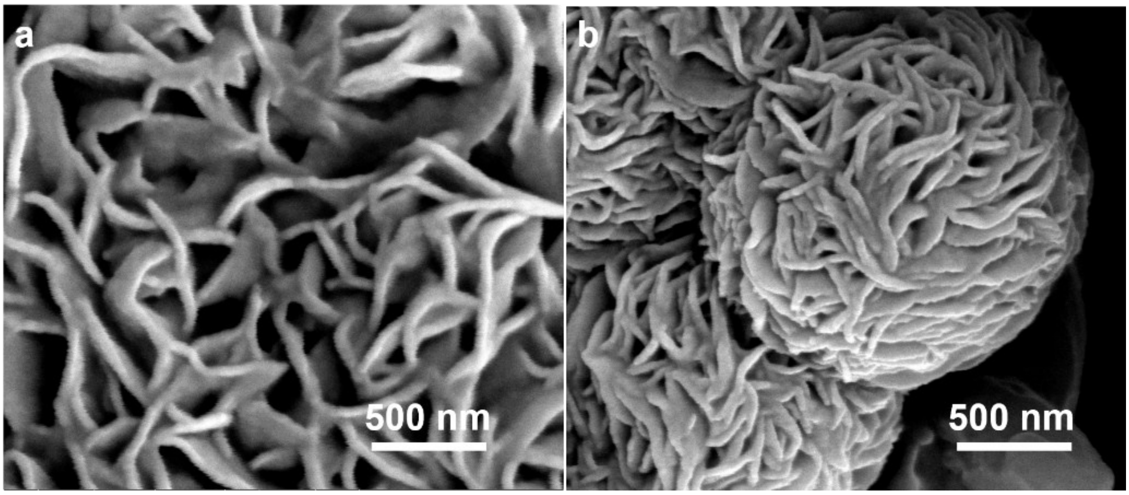

Figure S6 SEM images of $Ru_xSe@MoS_2$ after a long-term HER test.

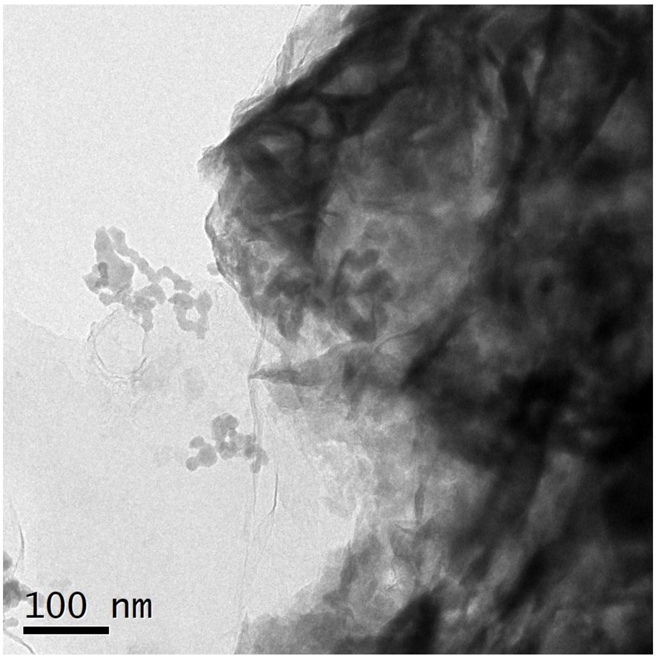

Figure S7 TEM images of $Ru_xSe@MoS_2$ after a long-term HER test.

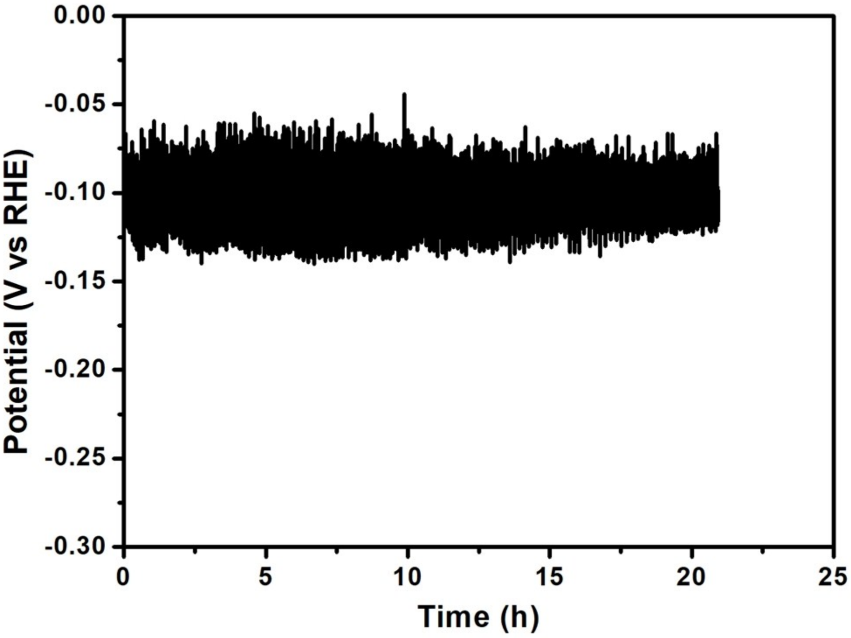

Figure S8 Time-dependent potential curves of commercial 20% Pt/C catalyst operated at a current density of -20 mA cm^{-2}

Table S1 The overpotential at the current density of 10 mA/cm^2, Tafel slope for MoS$_2$-based HER electrocatalysts in alkaline media.

Catalysts	η@10 mA cm^{-2} (mV)	Tafel slope (mV dec^{-1})	Ref.
MoS$_2$ intercalated with Co(OH)$_2$ nanoparticles	89	53	ACS Nano, 2018, 12:4565-4573
Nickel Hydr(oxy)oxide nanoparticles on metallic MoS$_2$ nanosheets	73	75	Adv. Sci., 2018, 5:1700644
Ni(OH)$_2$/MoS$_2$ heterostructure	80	60	Nano Energy, 2017, 37:74-80
Ni-doped MoS$_2$ nanosheets	98	60	Energy Environ. Sci., 2016, 9:2789-2793
Ni(OH)$_2$/MoS$_2$ heterostructures	227	105	Nanoscale, 2018, 10:19074-19081
Amorphous nickel-cobalt complexes hybridized with 1T-phase MoS$_2$	70	38.1	Nat. Commun., 2017, 8:15377
Aligned MoS$_2$/Ni$_3$S$_2$ Nanoarrays on Ni foam	76	56	ACS Appl. Mater. Interfaces, 2018, 10:1752-1760
MoS$_2$/Ni$_3$S$_2$ Heterostructures	110	50	Angew. Chem. Int. Ed. Engl., 2016, 55:6702-

			6707
MoS_2 nanosheet arrays vertically aligned on graphene-mediated 3D Ni networks	>600	98	Adv. Funct. Mater., 2014, 24:6123-6129
Interlaced NiS_2-MoS_2 Nanoflake-Nanowires	~120	70	J. Mater. Chem. A, 2016, 4:13439-13443
MoS_2-NiCo LDH hybrid	78	76.6	Joule, 2017, 1:383-393
Co_3O_4@MoS_2 Heterostructures	207	59.5	J. Mater. Chem. A, 2018, 6:2067-2072
Ni−Fe-LDH−MoS_2 nanohybrids	>330	67	ACS Energy Lett., 2018, 3:952-960
MoS_2−Ni_3S_2 Heteronanorods	98	61	ACS Catal., 2017, 7:2357-2366
NiS-$Ni(OH)_2$@MoS_{2-x}	226	81	Adv. Funct. Mater., 2016, 26, 7386
CoS-$Co(OH)_2$@MoS_{2-x}	143	68	